Molecular Orbital Calculations of Octahedral Molybdenum Cluster Complexes with the DV−Xα Method

Hideo Imoto* and Taro Saito

Department of Chemistry, School of Science, The University of Tokyo, Hongo, Tokyo, 113, Japan

Hirohiko Adachi

Department of Material Science, Kyoto University, Yoshidahonmachi, Sakyoku, Kyoto, 606-01, Japan

Received June 8, 1994[⊗]

Molecular orbital calculations with DV−Xα (discrete-variational Xα) method have been performed for $[Mo_6X_8(PH_3)_6]$ (X = S and Se). The calculated electronic spectra exhibit good agreements with the experimental spectra of the corresponding real compounds $[Mo_6X_8(PEt_3)_6]$. The calculated energies of 3d(Mo), 2p(P), and 2p(S) are within 1.3 eV of the observed values by XPS of the corresponding real compounds. The results of the calculations show large mixing of the 4d(Mo) orbitals with 3p(S) and 4p(Se) orbitals. The principal factors that determine the relative energies of the valence orbitals are the three types of interactions: (1) M−L, (2) M−M, and (3) L−L where M denotes the 4d(Mo) orbitals and L the p orbitals of the ligands. The contributions of these interactions are in the order of 1 > 2 > 3. The existence of the effect of interaction 3 is consistent with the observed "matrix effect". The stabilization of the 4d(Mo) orbitals by the metal−metal bonding causes the lowering of 4d(Mo) orbitals, and leads to the larger mixing of the metal orbitals and ligand orbitals. Similar calculation for $[Mo_6Cl_8(PH_3)_6]^{4+}$ shows smaller mixing of metal orbitals with bridging ligand orbitals, but larger mixing with the terminal ligand orbitals.

Introduction

The electronic structures of octahedral molybdenum clusters, $Mo_6Cl_8^{4+}$ and Mo_6S_8, have been the subjects of many papers.[1−7] Especially the sulfide cluster has been repeatedly studied because it is the structural unit of the superconducting Chevrel phases. However, the results of the calculations do not agree well with each other. In some of the results, the molybdenum 4d orbitals have much higher energies than the valence orbitals of ligands, and nearly pure molybdenum 4d orbitals make metal−metal bonding orbitals. Other results show the metal orbitals are mixed with ligand orbitals in a large extent and suggest that the Mo_6S_8 unit is a group of 14 atoms bonded covalently with each other, and the electronic structure is inevitably complicated. Because the Mo_6S_8 unit is hypothetical, it is impossible to determine experimentally which results are more plausible. Recently, molecular analogues of the Chevrel compounds, $[Mo_6X_8(PEt_3)_6]$ (X = S (**1**) and Se (**2**)), have been prepared and their visible spectra and XPS (X-ray photoelectron spectroscopy) have been measured.[8] These spectra are good tests of the validity of the molecular orbital calculations. Since the organic parts of the real compounds give an unnecessary burden on the MO calculations by destroying the O_h symmetry, we have used model compounds $[Mo_6X_8(PH_3)_6]$ (X = S (**3**), Se (**4**)) for the calculations. The assumed structure of **3** is shown in Figure 1.

The DV−Xα method (discrete variational X-α method)[9,10] with the SCC (self-consistent charge) approximation[11,12] is simple enough to be applied to such large cluster compounds. The DV−Xα method has been applied to carbonyl cluster complexes,[13,14] rhenium chloride clusters,[15] and transition-metal dinuclear complexes with various ligands.[16−19] The results of these calculations have shown good agreements with photo-

[⊗] Abstract published in *Advance ACS Abstracts,* April 1, 1995.

(1) Cotton, F. A.; Haas, T. E. *Inorg. Chem.* **1964**, *3*, 10.
(2) Cotton, F. A.; Stanley, G. G. *Chem. Phys. Lett.* **1978**, *58*, 450.
(3) Wooley, R. G. *Inorg. Chem.* **1985**, *24*, 3519.
(4) Seifert, G.; Groβmann, G. Müller, H. *J. Mol. Struct.* **1980**, *64*, 93.
(5) Nohl, H.; W. Klose; Andersen, O. K. *Super Conductivity in Ternary Compounds, I*; Fisher, Ø., Maple, M. B., Eds; Springer Verlag: Berlin, 1982; p 165.
(6) Le Beuze, L.; Makhyoun, M. A.; Lissillour, R.; Chermette, H. *J. Chem. Phys.* **1982**, *76*, 6060.
(7) Hughbanks, T; Hoffmann, R. *J. Am. Chem. Soc.* **1983**, *105*, 1150.
(8) (a) Saito, T.; Yamamoto, N.; Yamagata, T.; Imoto, H. *J. Am. Chem. Soc.* **1988**, *110*, 1646. (b) Saito, T.; Yamamoto, N.; Nagase, T; Tsuboi, T.; Kobayashi, K.; Yamagata, T.; Imoto, H. Unoura, K. *Inorg. Chem.* **1990**, *29*, 764.
(9) Slater, C. J. *The Calculation of Molecular Orbitals*; John Wiley & Sons: New York, 1979; p 52.
(10) Averill, F. W.; Ellis, D. E. *J. Chem. Phys.* **1973**, *59*, 6412 and references therein.
(11) Rosén, A.; Ellis, D. E.; Adachi, H.; Averill, F. W. *J. Chem. Phys.* **1976**, *65*, 3629.
(12) (a) Adachi, H.; Tsukada, M.; Satoko, C. *J. Phys. Soc. Jpn.* **1978**, *45*, 875. (b) Satoko, C.; Tsukada, M.; Adachi, H. *J. Phys. Soc. Jpn.* **1978**, *45*, 1333. (c) Adachi, H.; Shiokawa, S.; Tsukada, M.; Satoko, C.; Sugano, S. *J. Phys. Soc. Jpn.* **1979**, *47*, 1528.
(13) (a) Delley, B.; Manning, M. C.; Ellis, D. E.; Berkowitz, J.; Trogler, W. C. *Inorg. Chem.* **1982**, *21*, 2247. (b) Holland, G. F.; Ellis, D. E.; Trogler, W. C. *J. Am. Chem. Soc.* **1986**, *108*, 1884. (c) Holland, G. F.; Ellis, D. E.; Tyler, D. R.; Gray, H. B.; Trogler, W. C. *J. Am. Chem. Soc.* **1987**, *109*, 4276. (d) Trogler, W. C. *Acc. Chem. Res.* **1990**, *23*, 239.
(14) (a) Casarin, M.; Ajò, D.; Granozzi, G.; Tondello, E.; Aime, S. *Inorg. Chem.* **1985**, *24*, 1241. (b) Casarin, M.; Ajò, D.; Lentz, D.; Bertoncello, R.; Granozzi, G. *Inorg. Chem.* **1987**, *26*, 465. (c) Casarin, M.; Gulino, A.; Lentz, D.; Michael-Shulz, H.; Vittadini, A. *Inorg. Chem.* **1993**, *32*, 1383.
(15) Trogler, W. C.; Ellis, D. E.; Berkowitz, J. *J. Am. Chem. Soc.* **1979**, *101*, 5896.
(16) Manning, M. C.; Holland, G. F.; Ellis, D. E.; Trogler, W. C. *J. Phys. Chem.* **1983**, *87*, 3083.
(17) (a) Casarin, M.; Ajò, D.; Vittadini, A.; Ellis, D. E.; Granozzi, G.; Bertoncello, R.; Osella, D. *Inorg. Chem.* **1987**, *26*, 2041. (b) Casarin, M.; Vittadini, A.; Vrieze, K.; Muller, F.; Granozzi, G.; Bertoncello, R. *J. Am. Chem. Soc.* **1988**, *110*, 1775. (c) Bertoncello, R.; Casarin, M.; Dal Colle, M.; Granozzi, G.; Mattogno, G.; Muller, F.; Russo, U.; Vrieze, K. *Inorg. Chem.* **1989**, *28*, 4243.

0020-1669/95/1334-2415$09.00/0

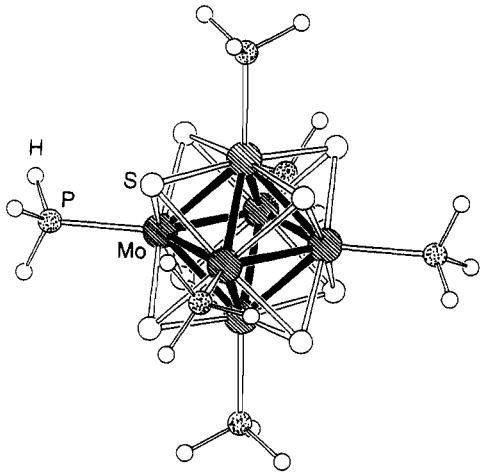

Figure 1. Assumed structure of $Mo_6S_8(PH_3)_6$.

electron and/or electronic spectra, and we expect that the method will give reliable results also for the molybdenum cluster compounds.

Experimental Section

MO Calculations. The molecular orbitals were calculated by the DV−Xα method with the SCC approximation.[9-12] All calculations were performed on a Mips RS3230 computer. The exchange parameter α was taken to be 0.70 in all calculations. Numerical atomic orbitals from atomic Hartree−Fock−Slater calculations were used as basis functions. The radial functions of the AOs were calculated at the points of the distance $r = r_n\exp(-k/32)$ ($k = 0.299$) from the nucleus, where r_n was 30 au for non-hydrogen atoms, and 20 au for hydrogen atoms. For the calculation of higher AOs, additional well potentials were added,[10] which were constant for $r < r_w$ and proportional to $1/r$ for $r > r_w$. The well potentials with r_w in parentheses were −0.1 au (2.1 Å) for 5p(Mo), −0.4 au (1.9 Å) for 3d(S), and −0.3 au (1.9 Å) for 3d(P) and 4d(Se). All orbitals through 5p were included for Mo, through 4d for Se, and through 3d for S, P, and Cl. Only the 1*s* orbital was used for H. The sampling points for the numerical integration of the matrix elements were distributed according to the method described in ref 10. The number of the sampling points were 500 000 for whole molecules and 200 000 for fragments (Mo_6 and Mo_6S_8).[20] The Coulomb potential was approximated by using the sum of the spherical atomic potentials. After the MOs were obtained as the solution of secular equations, the electron population on each AO was calculated and the values were used for the next calculation of the AOs. The process was cycled until the transfer of the electron by the population analysis was less than 0.0001 for all AOs (SCC = self-consistent charge method). For the calculation of the populations on AOs of **3**, both the Mulliken and Löwdin methods[21] were examined. Mulliken population analysis gave negative populations for 5p(Mo), 3d(S), and 3d(P) orbitals. Because the results obtained by the SCC process with Löwdin population analysis for **3** gave 0.05% lower total energy than that obtained with Mulliken population analysis, the former analysis was adopted for all calculations. However, the differences of the results obtained by the two methods were trivial.

The geometries of **3** and **4** were taken from the averaged values of **1** and **2**, respectively. The geometrical data for a hypothetical compound $[Mo_6Cl_8(PH_3)]^{4+}$ were from the real compounds $M[Mo_6Cl_{14}]$ and $[Mo_6Cl_{12}(PBu_3)_2]$.[22,23] The assumed bond distances in Å were as follows: Mo−Mo = 2.663, Mo−S = 2.445, Mo−P = 2.527 for **3**; Mo−Mo = 2.703, Mo−Se = 2.560, Mo−P = 2.543 for **4**; Mo−Mo = 2.616, Mo−Cl = 2.473, and Mo−P = 2.619 for $[Mo_6Cl_8(PH_3)_6]^{4+}$. The P−H distances of the phosphine ligands were set at 1.40 Å, and the angles Mo−P−H, at 114.63°.

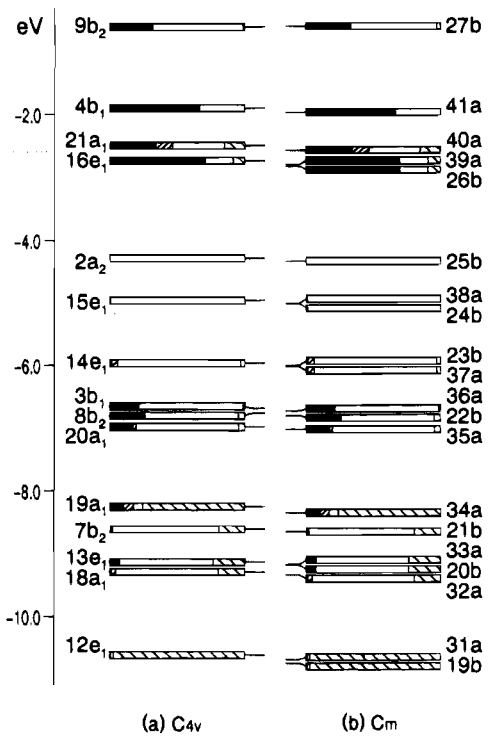

Figure 2. Electronic levels of $MoS_4(PH_3)$ (a) in the C_{4v} symmetry with the approximation described in the text and (b) the C_s symmetry.

PH_3 Group. Though the essential parts of the cluster molecules **1** and **2** had the O_h symmetry, the whole molecules did not have exact O_h symmetry due to the 3-fold symmetry of the phosphine ligands. The use of their true symmetry (C_s, C_i, or C_1) would make the discussion of the molecular orbitals very unclear and would require a very long computational time. Therefore, we applied the O_h symmetry for the molecular orbital calculation of **3** and **4** by treating the set of the 1*s* orbitals of the three hydrogen atoms of a phosphine in a special way: the hydrogen orbitals (φ_{H1}, φ_{H2}, and φ_{H3}) were combined to form three symmetry-adapted orbitals, $\varphi_A = \varphi_{H1} + \varphi_{H2} + \varphi_{H3}$, $\varphi_B = 2\varphi_{H1} - \varphi_{H2} - \varphi_{H3}$, $\varphi_C = \varphi_{H2} - \varphi_{H3}$, and it was assumed that φ_B and φ_C orbitals were equivalent. This approximation is equivalent to the neglect of the interactions of the hydrogen orbitals with the a_{2g}, e_u, t_{2u}, and t_{2g} symmetry-adapted orbitals of other atoms. However, the important interactions for hydrogen orbitals were those with the s and p orbitals of the bonded phosphorus atom and the s orbitals of other hydrogen atoms in the same phosphine ligand, and they were correctly included in the calculation. We confirmed that the DV−Xα calculation for a fraction, $[MoS_4(PH_3)]^{5-}$, with an approximation equivalent to this gave very similar results to those obtained without the approximation (Figure 2).

Calculation of Electronic Absorption Spectra. The transition energies were calculated by the transition-state method with 200 000 sampling points. Both non-spin and spin-polarized calculations were performed for the transitions $10t_{2u} \rightarrow 17e_g$ and $26t_{1u} \rightarrow 17e_g$ of **3** and $13t_{2u} \rightarrow 20e_g$ and $32t_{1u} \rightarrow 20e_g$ of **4**, and the results agreed within 0.01 eV. Therefore, the transition energies were calculated without spin-polarization. The absorption intensities were obtained as oscillation strength. A part of the pas program[24] was used for the calculation of

(18) Rizzi, G. A.; Granozzi, G.; Casarin, M.; Basato, M. *Organometallics* **1987**, *6*, 2536.
(19) Rizzi, G. A.; Casarin, M.; Tondello, E.; Piraino, P.; Granozzi, G. *Inorg. Chem.* **1987**, *26*, 3406.
(20) The DV−Xα calculations of $Mo_6X_8(PH_3)_3$ (X = S and Se) were performed with both 200 000 and 500 000 sampling points. The resulting energies of the orbitals between 0 and −100 eV agreed within 0.02 eV for X = S and 0.03 eV for X = Se, and we concluded 200 000 points were enough for our calculations.
(21) (a) Löwdin, P.-O. *Adv. Quantum Chem.* **1970**, *5*, 185. (b) Szabo, A.; Ostlund, N. S. *Modern Quantum Chemistry*, Revised 1st ed.; McGraw-Hill: New York, 1989; p 149.
(22) Potel, M.; Perrin, C.; Sergent, *M. Mater. Res. Bull.* **1986**, *21*, 1239.
(23) Saito, T.; Nishida, ; Yamagata, T.; Yamagata, Y; Yamaguchi, Y. *Inorg. Chem.* **1986**, *25*, 1111.
(24) (a) Adachi, H.; Taniguchi, K., *J. Phys. Soc. Jpn.* **1980**, *49*, 1944. (b) Ishikawa, H. Private communication.

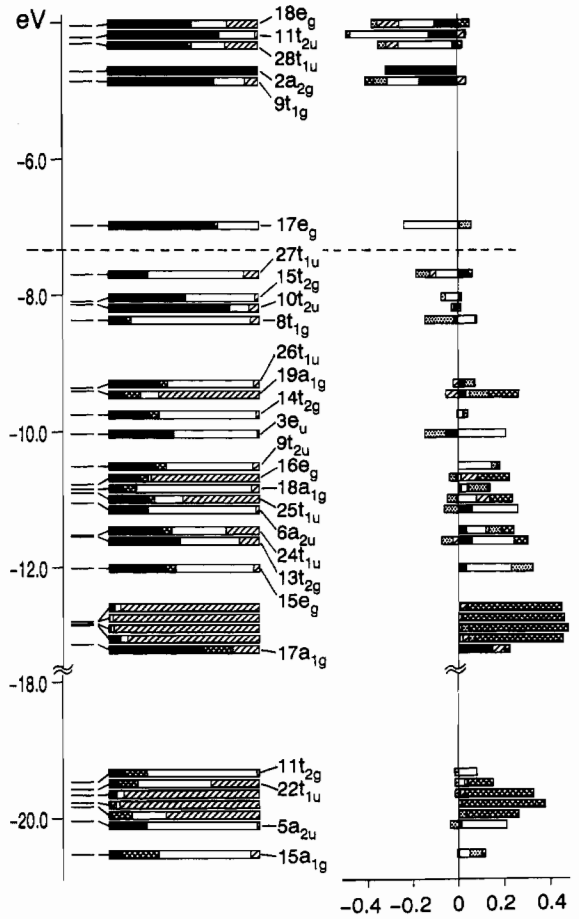

Figure 3. Electronic levels and overlap populations of $Mo_6S_8(PH_3)_6$. Short horizontal lines just right of the vertical axis indicate the energies of the levels. The left strips show the AO compositions of each MO: black, 4d(Mo); cross-hatched, 5p5s(Mo); white, 3s3p(S); hatched, 3s3p-(P) and 1s(H). The right strips show the overlap populations: black, 4d(Mo)-4d(Mo); white, 4d(Mo)−3x(S); hatched, 4d(Mo)−3x(P); dotted, 3x(S)−3x(S), 3x(S)−3x(P), and 3x(P)−3x(P) where x is p for levels higher than −14 eV and s for those lower than −18 eV.

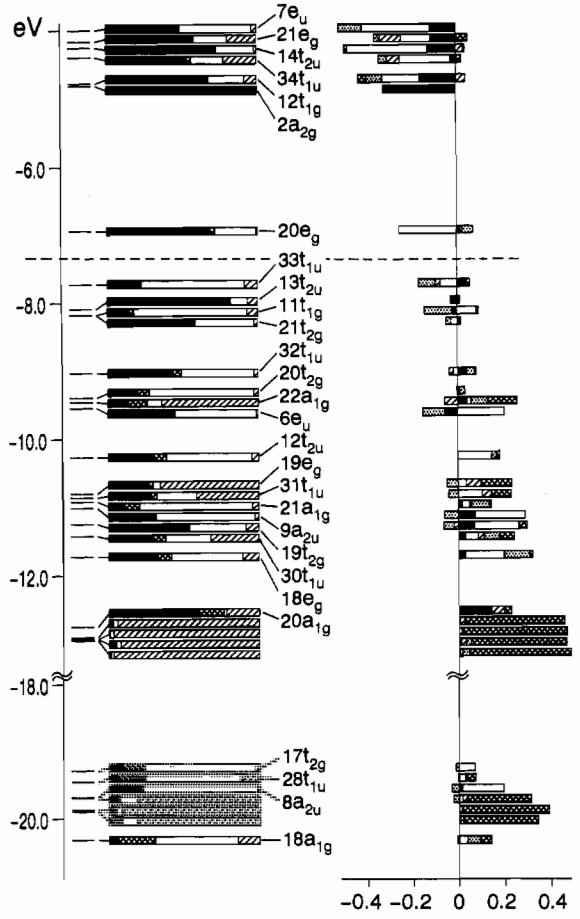

Figure 4. Electronic levels and overlap populations of $Mo_6Se_8(PH_3)_6$. Short horizontal lines just right of the vertical axis indicate the energies of the levels. The left strips show the AO compositions of each MO: black, 4d(Mo); cross-hatched, 5s5p(Mo); white, 4s4p(Se); hatched, 3s3p(P) and 1s(H). The right strips show the overlap populations; black, 4d(Mo)−4d(Mo); white, 4d(Mo)−4x(Se); hatched, 4d(Mo)−3x(P); dotted, 4x(Se)−4x(Se), 4x(Se)−3x(P), and 3x(P)−3x(P) where x is p for levels higher than −13 eV and s for those lower than −14 eV.

oscillation strength. The number of the sampling points used for the calculation of the oscillation strength was 1 million.

Results

Energy Levels. The calculated one-electron energy level diagrams for **3** and **4** are shown in Figures 3 and 4, respectively. They are very similar and we will describe only the important MOs of the former here. The LUMO of **3** is the $17e_g$ orbital consisting mainly of 4d(Mo) and 3p(S) orbitals and has a weak Mo−S antibonding nature. The dominant component of the HOMO ($27t_{1u}$) is the 3p(S) orbitals. The second HOMO ($15t_{2g}$) has a larger contribution of 4d(Mo) orbitals though its major component is the 3p(S) orbital. The third HOMO ($10t_{2u}$) is the highest occupied orbital that contains the 4d(Mo) orbitals as the principal component. The contour maps of these orbitals are drawn in Figure 5.

Visible and Near Infrared Spectra. The calculated electronic spectra of **3** and **4** are shown in Figures 6 and 7 with the observed spectra of **1** and **2**. They reproduce the two characteristic absorptions of the real spectra below 20 000 cm^{-1}. The absorptions of **1** and **2** observed around 9000 cm^{-1} are assigned to the $t_{2u} \rightarrow e_g$ (=LUMO) transition ($10t_{2u} \rightarrow 17e_g$ for **1** and $13t_{2u} \rightarrow 20e_g$ for **2**). Both of the initial and the final MOs of these transitions consist mainly of 4d(Mo) orbitals, and they are, therefore, charge-transfer transitions from metals to metals. Other absorptions observed around 20 000 cm^{-1} are assigned to the $t_{1u} \rightarrow e_g$ (=LUMO) transition ($26t_{1u} \rightarrow 17e_g$ for **1** and $32t_{1u} \rightarrow 20e_g$ for **2**). The initial MO of these transitions is a mixture of 4d(Mo) and chalcogen p orbitals.

The absorptions around 9000 cm^{-1} of **1** and **2** and one around 20 000 cm^{-1} of **2** split into two components in real compounds. If we neglect the possibility of the spin forbidden transition, both of the $t_{2u} \rightarrow e_g$ and $t_{1u} \rightarrow e_g$ transitions generate two excited states, $^1T_{1u}$ and $^1T_{2u}$, which is consistent with the observed splittings. Though it should be possible in principle to calculate the splitting,[25] our attempts to evaluate the value have been unsuccessful.[26]

Above 25 000 cm^{-1}, the agreement between the calculated transitions and the observed absorptions is not so good as in the lower energy region. The transition expected around 27 000 cm^{-1} in both **3** and **4** may be one of the components of the strong absorption band observed higher than 30 000 cm^{-1}. This discrepancy suggests that the gap between LUMO and the

(25) Ziegler, T.; Rauk, A.; Baerends, E. J. *Theoret. Chim.* **1977**, *43*, 261.

(26) For the calculations of the exact transition energies of the spatial multiplets, the DV−Xα calculations without the symmetry restriction are required. However, if the symmetry were ignored, the system would be too large to be calculated with our computer. Therefore, we attempted to obtain the approximate values of these splittings by evaluating the Coulomb energies between the electrons occupying the initial and final orbitals. The results were strongly dependent on the approximation method, and the observed values (ca. 1000 cm^{-1} = 0.12 eV) were not reproduced.

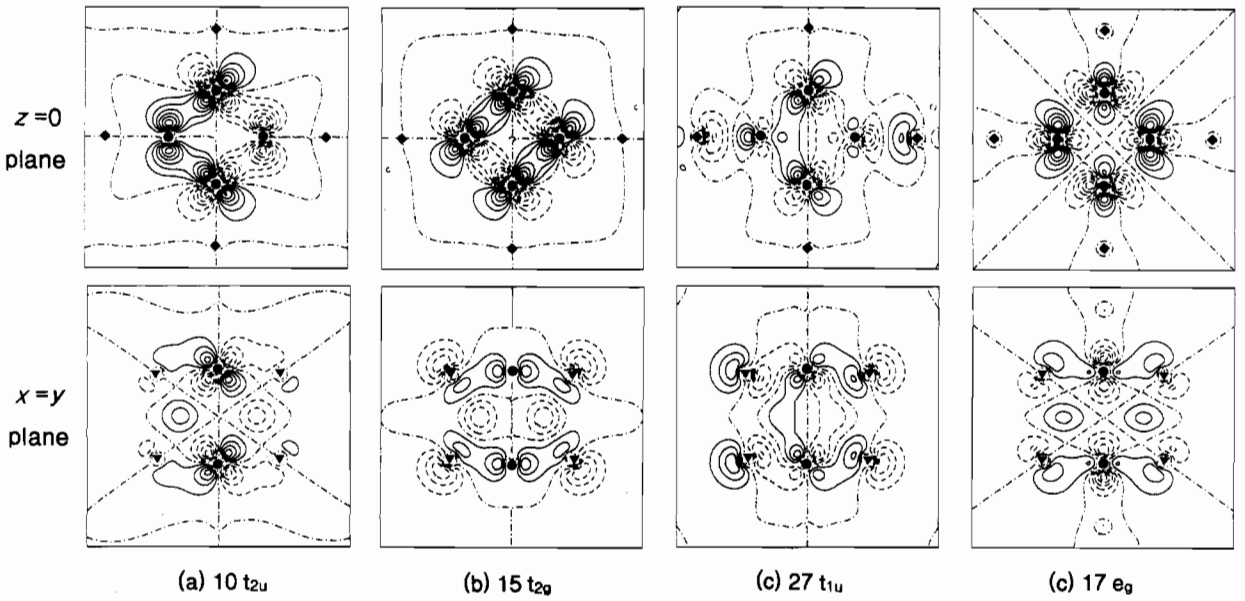

Figure 5. Contour maps of the molecular orbitals of $Mo_6S_8(PH_3)_6$: (a)$10t_{2u}$, (b)$15t_{2g}$, (c)$27t_{1u}$ (HOMO), and (d)$17e_g$ (LUMO). For a, b, and c, the contours on the xy plane and on a diagonal plane ($x = y$) of an orbital among three degenerate orbitals are shown, respectively. For d, the contour on the $z = 0$ plane of the $x^2 - y^2$ type orbital and the contour on the diagonal plane ($x = y$) of the $3z^2 - r^2$ type orbital are shown.

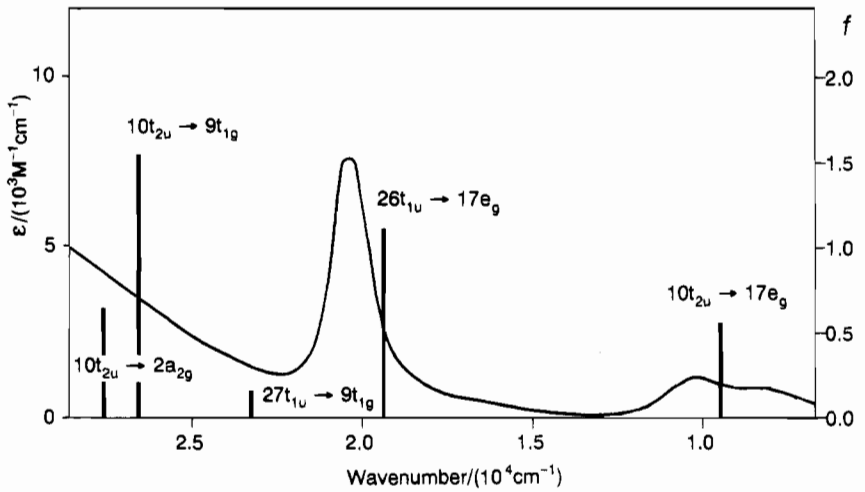

Figure 6. Observed visible and near-infrared spectrum of $Mo_6S_8(PEt_3)_6$, and the calculated oscillation strengths for $Mo_6S_8(PH_3)_6$.

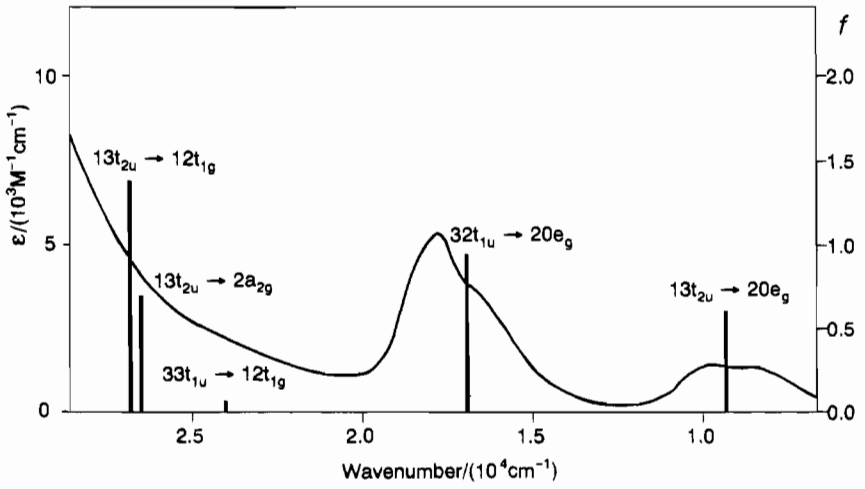

Figure 7. Observed visible and near-infrared spectrum of $Mo_6Se_8(PEt_3)_6$, and the calculated oscillation strengths for $Mo_6Se_8(PH_3)_6$.

metal−metal antibonding orbital groups are a little larger than the calculated values.

XPS. The calculated energies of the levels for the ground state for model compounds **3** and **4** with the XPS binding energies for **1** and **2** are in Table 1. The calculated values except for the 3d(Se) orbital are within 1.3 eV of the observed binding energies. The calculation by the transition-state method gave much lower values than the observed values.[27]

Table 1. Comparison of the Calculated Energies of the Levels and Observed XPS for $Mo_6X_8(PR_3)_6$

compound[a]	orbital	enerty (eV) calcd[b]	obsd[c]
$Mo_6S_8(PR_3)_6$	3d(Mo)	229.0	229.1[d]
	2p(S)	158.9	161.1
	2p(P)	129.3	130.6
$Mo_6Se_8(PR_3)_6$	3d(Mo)	228.8	229.0[e]
	3d(Se)	57.0	53.8
	2p(P)	129.3	130.6

[a] R is H for calculated values, and C_2H_5 for observed values. [b] The energies of the corresponding levels in the ground state. [c] Reference 8b. [d] The weighted average of 227.8 eV ($3d_{5/2}$) and 231.0 eV ($3d_{3/2}$). [e] The weighted average of 227.8 eV ($3d_{5/2}$) and 230.8 eV ($3d_{3/2}$).

Table 2. Numbers of Symmetry-Adapted Orbitals of Each Fragment of $Mo_6S_8(PH_3)_6$

	4d(Mo)	3p(S)[a]	3p(P)[b]
a_{1g}	1	1 (B)	1
a_{2g}	1	0	0
a_{2u}	1	1 (A)	0
e_g	2	1 (B)	1
e_u	1	1 (A)	0
t_{1g}	1	1 (A)	0
t_{1u}	2	2 (A + B)	1
t_{2g}	2	2 (A + B)	0
t_{2u}	2	1 (B)	0

[a] The A and B in parentheses mean antibonding and bonding, respectively, when they are considered as MOs of the S_8 fragment. [b] The orbitals used mainly for P−H bonds are omitted.

Discussion

We will describe the electronic structures of $[Mo_6X_8(PH_3)_6]$ clusters based on the results of our calculations. Our goal is to extract the main factor that determines the MO energies. Since $[Mo_6S_8(PH_3)_6]$ and $[Mo_6Se_8(PH_3)_6]$ have very similar electronic structure as shown in Figures 3 and 4, we will discuss only the former. We will first consider the orbitals of an Mo_6 cluster, then the interaction between the Mo_6 cluster and the sulfido ligands, and finally the effect of the coordination of the phosphine ligands. The numbers of the symmetry-adapted orbitals of each fragment are summarized in Table 2.

Orbitals of Mo_6 Fragment. The schematic shapes of the symmetry-adapted 4*d*(Mo) orbitals of a Mo_6 cluster are shown in Figure 8. Their energies and overlap populations are in Figure 10. For e_g, t_{1u}, t_{2g}, and t_{2u} symmetry, the fragment has two orbitals. The orbitals with the same symmetry mix with each other to yield a bonding MO and an antibonding MO as shown in Figure 10. When these orbitals interact with ligand orbitals (Figure 9), they can flexibly change their shapes by varying the mixing ratio to maximize the stabilization of the lowest MO. Therefore, the interaction with ligand orbitals enhances the separation of the energies of the orbitals of the same symmetry.

There is only one type of the 4d(Mo) orbitals for other representations. Among them, $9a_{1g}$ and $2a_{2u}$ are bonding orbitals, and $2a_{2g}$, $2e_u$, and $5t_{1g}$ orbitals are antibonding metal orbitals. The latter will be used for the stabilization of the 3p(S) orbitals except for the $5t_{1g}$ orbital that cannot interact with the 3p(S) orbitals due to its symmetry.

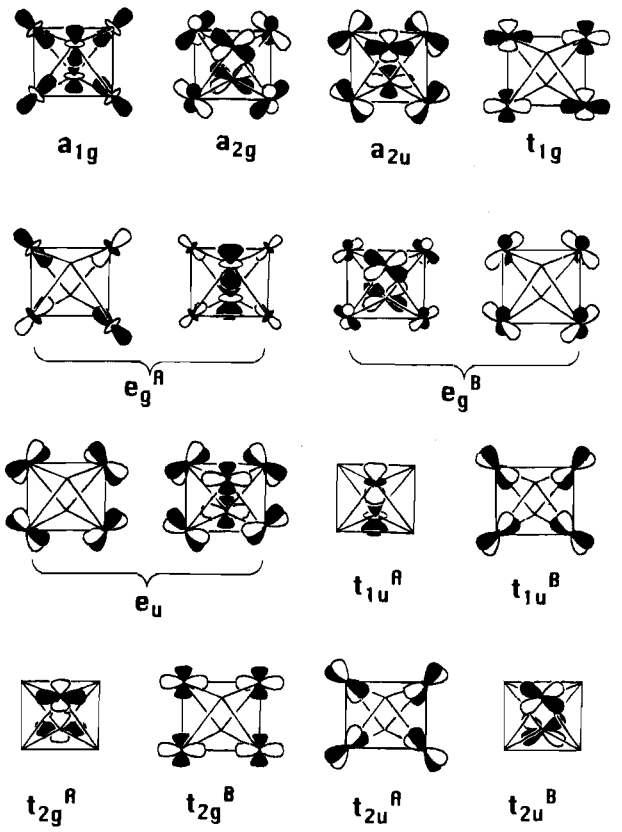

Figure 8. Schematic figures of the symmetry adapted molybdenum 4d orbitals in a Mo_6 cluster. For e_g, t_{1u}, t_{2g}, and t_{2u} orbitals, the orbital with higher energy has the superscript A, and the one with lower energy has the superscript B.

The $10a_{1g}$ orbital in Figure 10 is made mainly of 5s and 5p orbitals, and they are lifted to a higher energy by the interaction with the ligand orbitals.

Mo_6−S_8 Orbital Interaction. As indicated by the AO compositions of the valence orbitals between −8 and −14 eV (Figure 11), the 4d(Mo) orbitals and 3p(S) orbitals are not separated, but they are well mixed. If they were sufficiently separated, the order of the MOs would be easily interpreted: the 4d(Mo) orbitals that interact with 3p(S) orbitals would be strongly destabilized, and the order of other 4d(Mo) orbitals would be determined by the Mo−Mo interaction. However, in our results the 4d(Mo) orbitals and 3p(S) orbitals have similar energies and the energy levels must be interpreted in a different way.

In Figure 11, the center of the strip of the overlap populations of a level between −13 and −5 eV shifts smoothly from right to left as the energy of the level increases. Because the position of the center of the strip is proportional to the sum of the overlap populations of 4d(Mo)−4d(Mo), 4d(Mo)−3p(S), and 3p(S)−3p(S), the smooth shift means that the sum of these overlaps decreases as the energy of the level increases. In other words, the energy of a MO in this energy region is mainly determined by the sum of these three interactions and not by the AO composition of the MO.

The dimensions of these interactions are not equal. The distances of Mo−Mo, Mo−S, and S−S are approximately in the ratio of $1:1:2^{1/2}$. The radius of the 3p(S) orbital is larger than that of the 4p(Mo) orbital, and the strength of the interaction is expected to be in the order of 4d(Mo)−3p(S) > 4d(Mo)−4d(Mo) > 3p(S)−3p(S). This expectation is supported by the

(27) The reason why the transition-state calculations do not give more accurate values for binding energies of XPS, especially for the Se 3d orbital, has not been elucidated. One of the possible reason may be that the potential energy used in our calculation is not good enough for these calculations. The true potential for Se 3d electrons that is caused by the valence electrons should be more inhomogeneous than the sum of the spherical potential used for the calculation because the valence electrons are more concentrated along the bonds. Therefore, the true Coulomb energy caused by this potential will be larger, and the true orbital energy of the Se 3d orbital may be higher than the calculated one.

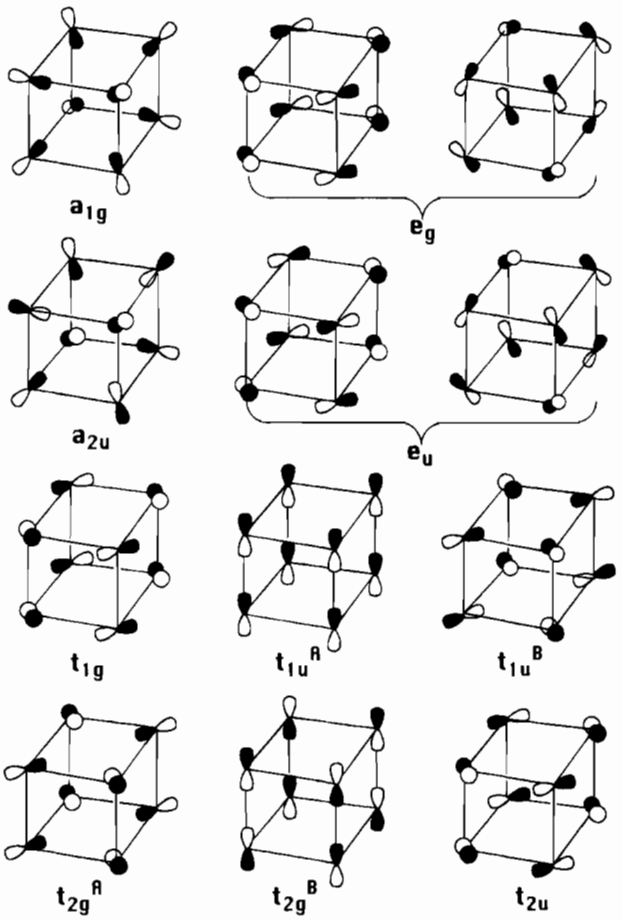

Figure 9. Schematic figures of the symmetry-adapted sulfur 3p orbitals in a cubic S_8 unit. For t_{1u} and t_{2g} orbitals, the orbital with higher energy has the superscript A, and the one with lower energy has the superscript B.

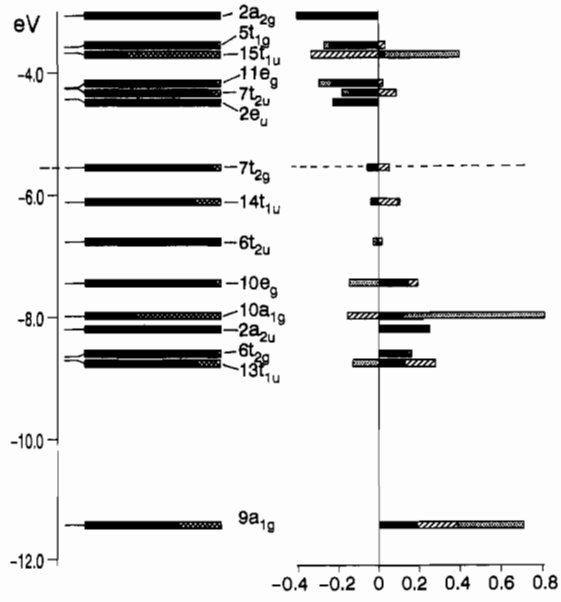

Figure 10. Electronic levels and overlap populations of a Mo_6 cluster. Short horizontal lines just right of the vertical axis indicate the energies of the levels. The left strips show the AO compositions of each MO: black, 4d; cross-hatched, 5p5s. The right strips show the overlap populations: black, 4d-4d; hatched, 4d-5s5p; dotted, 5s5p-5s5p.

calculated overlap populations in Figure 11. The 4d(Mo)−3p(S) interactions are most dominant in total, the 4d(Mo)−4d(Mo) interactions are next, and the 3p(S)−3p(S) interactions are the smallest. Though the 4d(Mo)−3p(S) overlap populations are

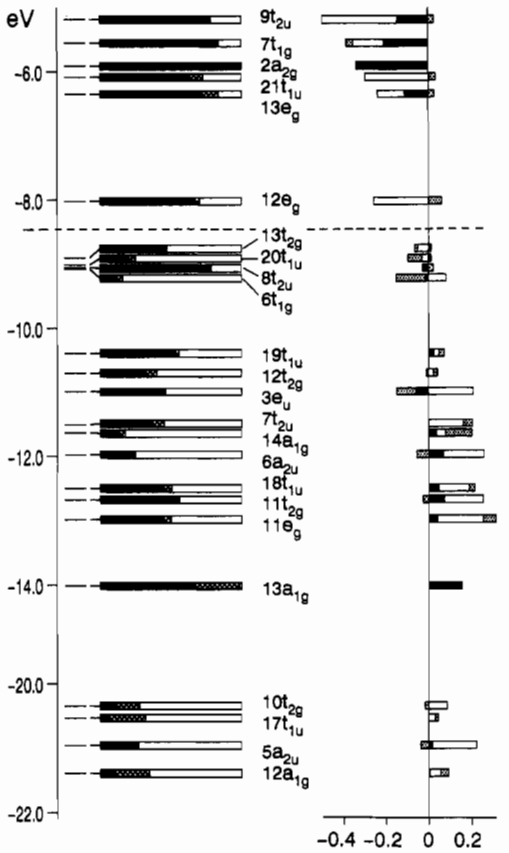

Figure 11. Electronic levels and overlap populations of a Mo_6S_8 cluster. Short horizontal lines just right of the vertical axis indicate the energies of the levels. The left strips show the AO compositions of each MO: black, 4d(Mo); cross-hatched, 5p5s(Mo); white, 3s3p(S). The right strips show the overlap populations: black, 4d(Mo)−4d(Mo); white, 4d(Mo)−3p(S); dotted, 3x(S)−3x(S) where x is p for levels higher than −15 eV and s for those lower than −20 eV.

the largest, they are still much smaller than those found in the usual covalent bonding as P−H bonds (Figure 3). Therefore, the 3p(S)−3p(S) interaction, which is supposed to be a weak interaction between nonbonded atoms, plays a nonnegligible role in determining the energy levels. For example, if there were no effect of the 3p(S)−3p(S) interactions, the $3e_u$ orbital (Figure 11), which has a strongly 4d(Mo)−3p(S) bonding nature, would have a lower energy than the $14a_{1g}$ orbital. The 3p(S)−3p(S) interaction destabilizes the former and stabilizes the latter, resulting the reverse of the order of the levels. This 3p(S)−3p(S) overlap is related to the matrix effect in M_6X_8 clusters. The matrix effect observed in Mo_6X_8 clusters suggests that ligand−ligand interaction is an important factor that determines the size of the metal cluster.[28]

The interaction between the 4d(Mo) orbitals and the 3s(S) orbitals is also observed for MOs above −22 eV as shown in Figure 11. Though the overlap populations between 4d(Mo) and 3s(S) are as large as those between 4d(Mo) and 3p(S), the effect of the interaction between 4d(Mo) and 3s(S) may be much weaker than the interaction between 4d(Mo) and 3p(S) because the energy difference between the orbitals is large. The weakness of the effect is indicated by the energy of the $6a_{2u}$ orbital. It is a 4d(Mo)−3p(S) bonding orbital but is a 4d(Mo)−3s(S) antibonding orbital at the same time. The overlap population of 3s(S)−4d(Mo) in the $6a_{2u}$ is −0.28, which is larger in magnitude than the overlap population between 3p(S)−4d(Mo) (0.19). However, the energy of the $6a_{2u}$ is low as if there were no effect of 3s(S)−4d(Mo) antibonding interaction.

(28) Corbett, J. D. *J. Solid State Chem.* **1981**, *37*, 335.

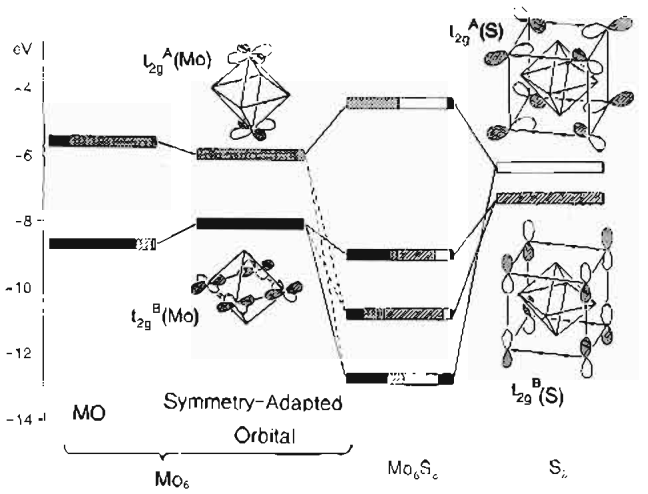

Figure 12. Interaction scheme of molybdenum and sulfur t_{2g} orbitals in Mo_6S_8. Each strip shows the AO compositions: black, t_{2g}^{B}–4d(Mo); coarsely dotted, t_{2g}^{A}–4d(Mo); gray, 5s5p(Mo); hatched, t_{2g}^{B}–3p(S); white, t_{2g}^{A}–3p(S); cross-hatched, 3s(S) and 4d(S).

Details of the Mo_6–S_8 Interaction. As described above, the energy diagram of the Mo_6S_8 unit is complex due to the interactions of 4d(Mo)–4d(Mo), 4d(Mo)–3p(S), and 3p(S)–3p(S). Another reason of the complexity is that most of the interaction between the 4d(Mo) and 3p(S) is of intermediate strength. Most of the symmetry-adapted orbitals in Figures 8 and 9 are not directed toward the surrounding atoms nor perpendicular to the directions of them. Among the possible combinations of the 4d(Mo) and the 3p(S) symmetry-adapted orbitals (Table 2), the σ-type interaction between 4d(Mo) and 3p(S) orbitals is found only in the combinations of a_{2u}, e_u, and t_{2g} (t_{2g}^{A}(Mo)-t_{2g}^{A}(S)) (Figures 8 and 9). Each of these interactions yields an antibonding orbital with higher content of the 4d(Mo) orbitals and a bonding orbital. The bonding and antibonding nature of these orbitals are indicated by the overlap populations between 4d(Mo) and 3p(S) orbitals (Figure 11). Other interactions between 4d(Mo) and 3p(S) orbitals in Table 2 are mixtures of σ-, π-, and δ-types and are weak. Therefore, we cannot treat the interactions between the 4d(Mo) and 3p(S) orbitals in the Mo_6S_8 cluster as the collection of the square planar MoS_4 complex but have to treat them as multicenter bonding.

For the a_{1g}, a_{2u}, e_u, and t_{1g} symmetry, each fragment of the Mo_6 and the S_8 has only one symmetry-adapted orbital (Table 2). The interaction of each pair of the symmetry-adapted orbitals yields an occupied bonding orbital and an unoccupied antibonding orbital except for the a_{1g} pair. The a_{1g} symmetry-adapted orbitals does not mix well, and the metallic orbital ($13a_{1g}$ in Figure 11) is much lower than the ligand orbital ($14a_{1g}$). While in mononuclear complexes in low oxidation states the metal d orbitals have usually higher energies than ligand orbitals, in the Mo_6S_8 cluster the $13a_{1g}$ is strongly stabilized by the metal–metal bonding.

The most complicated interaction occurs when both the S_8 and Mo_6 fragments have two types of symmetry-adapted orbitals as found for the t_{1u} and t_{2g} representations. The two-orbital–two-orbital interaction of these symmetry-adapted orbitals yields four MOs, and three of them are occupied.

The interaction scheme of the t_{2g} orbitals is shown in Figure 12. The interaction between the molybdenum orbital t_{2g}^{A} and the sulfur orbital t_{2g}^{A} is of the σ-type as described above and makes the main part of the lowest MO ($11t_{2g}$) and the highest MO ($14t_{2g}$). In addition, another molybdenum orbital (t_{2g}^{B}) also contributes to the lowest orbital through the bonding interaction between the two molybdenum orbitals. Therefore, the lowest orbital is a mixture of the Mo–S and the Mo–Mo bonding interaction. The next lowest orbital ($12t_{2g}$) is mainly made of the sulfur t_{2g}^{B} orbital. Both of the molybdenum t_{2g} orbitals combine with the sulfur orbital in a bonding mode, but the interaction between the molybdenum orbitals is slightly antibonding as indicated in Figure 11. The $13t_{2g}$ MO is a weakly-antibonding orbital of the sulfur t_{2g}^{B} and molybdenum t_{2g}^{B} orbitals, which is the HOMO of the Mo_6S_8 fragment, and becomes the second HOMO in **3** (Figure 3).

The interactions between the four t_{1u} orbitals are all weak. Among the two molybdenum and two sulfur t_{1u} orbitals, the sulfur t_{1u}^{A} orbital is relatively independent of other three, and is the main component of the $20t_{1u}$ MO (second HOMO), which becomes the HOMO of **3** (Figure 3). The lowest MO ($18t_{1u}$) is derived from the interaction between another sulfur orbital (t_{1u}^{B}) and the molybdenum t_{1u}^{B}, and the next lowest MO ($19t_{1u}$) is a bonding mixture of the molybdenum t_{1u}^{A} orbital with the antibonding combination of the components of the lowest MO. This MO becomes 26 t_{1u} in **3** (Figure 3), which is the initial orbital of the transition corresponding to the characteristic absorption observed around 20 000 cm^{-1} described above.

In the traditional view of the electronic structure of the Mo_6X_8 cluster, the molybdenum 4d orbitals make five bonding MOs in the order $a_{1g} < t_{1u} < t_{2g} < t_{2u} < e_g$. In the present study, the molybdenum orbitals, especially t_{1u} and t_{2g} orbitals, are strongly mixed with the sulfur orbitals. These orbitals split into more than two orbitals in our calculation. The molybdenum t_{1u} and t_{2g} orbitals in the previous studies correspond to the pairs of orbitals $18t_{1u}$–$19t_{1u}$ and $12t_{2g}$–$13t_{2g}$ in the present study (Figure 11), respectively. When we regard the average of the energies of these pairs as the metal orbital energy, the order of the metal orbitals is the same as the reported.

M_6S_8–$(PH_3)_6$ Interaction. As shown in Figure 3, the mixing of the phosphorus 3p orbitals and the metal 4d orbitals is not so strong as the mixing of the sulfur and metal orbitals. The $19a_{1g}$, $16e_g$, and $25t_{1u}$ MOs in Figure 3 are derived from the phosphine orbitals since they have conspicuously large contents of the phosphorus AOs (Figure 3). The coordination of the phosphine ligands leads to the electron transfer from the phosphorus atoms to the metal–sulfur cluster, and most of the occupied orbitals of the Mo_6S_8 cluster are destabilized. However, the metal a_{1g} orbital is stabilized by the incorporation of the phosphorus orbitals since the metal a_{1g} orbital is lower in energy than the phosphorus a_{1g} orbital.

An obvious effect of the phosphine coordination is the exchange of the HOMO and the second HOMO. The second HOMO of Mo_6S_8 cluster ($20t_{1u}$ in Figure 11) containing the radial 4d(Mo) orbital (t_{1u}^{A} in Figure 8) is destabilized by the phosphorus orbital to become the HOMO ($27t_{1u}$ in Figure 3).

Energy Difference between Metal Orbitals and Ligand Orbitals. The strong mixing of molybdenum 4d orbitals and chalcogen p orbitals found in our calculation is due to the small energy difference of the molybdenum 4d orbitals and the chalcogen p orbitals. Such small energy difference between ligand atoms and molybdenum atoms is partly due to the electron transfer from metal atoms to ligand atoms. Electron transfer causes the reduction of energy separation and has been stated as the principle of electronegativity equalization.[29] The total amount of the electron transferred from six Mo atoms to eight chalcogen atoms is 1.04 for Mo_6S_8 and 0.142 for Mo_6Se_8. A similar tendency has been reported for a series of molybdenum halide clusters $Mo_6X_8^{2+}$.[4] However, the amount of the electron transfer seems too small for the observed

(29) Sanderson, R. T. *Polar Covalence*; Academic Press: New York, 1983; p 37.

lowering of the metal 4d orbitals relative to the chalcogen orbitals. In fact, in a hypothetical mononuclear complex, Mo(SH)$_4$PH$_3$, the molybdenum 4d orbitals are not so much mixed with ligand orbitals as observed in the clusters and its energy is 1.7 eV higher than that of the highest sulfur 3p orbital (Figure 2). It has been proved by the UV photoelectron spectroscopy and electronic structure calculations that in a similar real molybdenum complex, Mo(S-*t*-Bu)$_4$, molybdenum 4*d* orbital is 1.33 eV higher than the highest occupied sulfur orbital.[30] The main reason for the low metal 4d orbitals in Mo_6X_8 cluster compounds is the stabilization of the metal d-orbitals by the metal−metal bonding. The 4d-orbitals of molybdenum atoms in a cluster interact with each other to make a "band" and the "bandwidth" is much larger than the energy difference between the metal orbital and ligand orbitals. The very low metal orbitals may be characteristic of the cluster compounds, and they make strong covalent bonds with ligand orbitals. Therefore, we can expect that the redox behavior of metal cluster compounds of the early transition metals, whose valence d-electrons occupy only the orbitals stabilized by the metal−metal bonding, is similar to mononuclear complexes in a higher oxidation state.

Comparison with a $Mo_6Cl_8^{4+}$ Cluster. While the mixing of 4d(Mo) orbitals and the p orbitals of the bridging ligands are very large in a Mo_6S_8 cluster, the mixing is expected to be smaller in $Mo_6Cl_8^{4+}$ clusters due to the lower energies of the 3p(Cl) orbitals. The calculated level diagram (Figure 13) for a hypothetical compound $[Mo_6Cl_8(PH_3)_6]^{4+}$ supports the expectation. If we neglect the MOs consisting mainly of the phosphine groups and the t_{1u} orbitals, the level diagram is simple. Between −17.1 and −15.7 eV, there are three MOs that consist mainly of 4d(Mo) orbitals. They are metal−metal bonding and metal−ligand antibonding orbitals. The ligand orbitals have energies between −20.8 and −18.0 eV, and most of them, especially those with lower energies, contain the 4d(Mo) orbitals in a bonding mode. These results are what we expect for a system with metal levels in higher energy and ligand levels in lower energy.

The large mixing of the t_{1u} orbitals is not the mixing of the 4d(Mo) and 3p(Cl) orbitals but of the 4d(Mo) and 3p(P) orbitals. The $(PH_3)_6$ fragment has three symmetry-adapted orbitals, a_{1g}, e_g, and t_{1u}, having lobes directed toward the molybdenum atoms. The a_{1g} 4d(Mo) orbital has a much lower energy and does not have a strong interaction with the phosphine a_{1g} orbital. On the other hand, the energy of the e_g 4d(Mo) orbital level is located too high to interact with the corresponding phosphine orbital. Only the t_{1u} orbital among the 4d(Mo) orbitals has a suitable energy to interact well with the phosphine orbitals. In the chloro-bridged clusters, the contribution of the terminal ligands is more important than in the sulfido-bridged clusters.

Concluding Remarks. The results of our DV−Xα calculations of $[Mo_6X_8(PH_3)_6]$ (X = S, Se) show very large mixing of metal *d* orbitals and chalcogen *p* orbitals (extensive mixing model) and are quite different from some of the previous results that gave MOs consisting almost of 4d(Mo) orbitals (isolated metal-orbital model). Our calculations of the electronic spectra have shown good agreement with the observed spectra, which supports the extensive mixing model. However, the isolated metal-orbital model might also give similar results for the electronic spectra. Though the two models appears very different, it is not easy to determine experimentally which model is more probable.

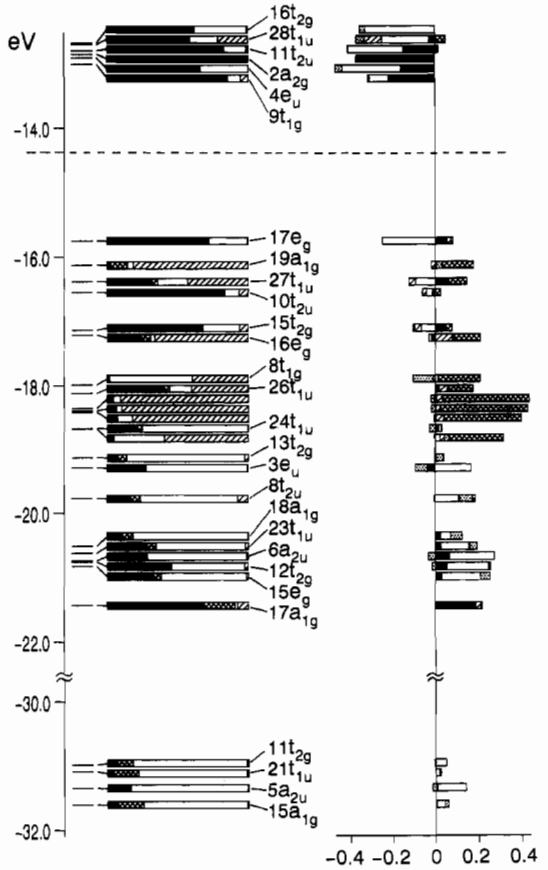

Figure 13. Electronic levels and overlap populations of $[Mo_6Cl_8(PH_3)_6]^{4+}$. Short horizontal lines just right of the vertical axis show the energies of the levels. The left strips show the AO compositions of each MO: black, 4d(Mo); cross-hatched, 5p5s(Mo); white, 3s3p(Cl); hatched, 3s3p(P) and 1s(H). The right strips show the overlap populations: black, 4d(Mo)−4d(Mo); white, 4d(Mo)−3x(Cl); hatched, 4d(Mo)−3x(P); dotted, 3x(Cl)−3x(Cl), 3x(Cl)−3x(P), and 3x(P)−3x(P) where x is p for levels higher than −22 eV and s for those lower than −30 eV.

The two models give different pictures for the reactivity of the oxidized clusters though we cannot estimate exact reactivity from electronic structure calculations of the ground states. The isolated metal-orbital model expects the oxidized cluster with the electron hole on the molybdenum atoms, and it suggests that the cluster may not be very reactive because the molybdenum atoms are guarded well by the ligands. By contrast, the extensive mixing model suggests that the electron hole is delocalized not only over the metal atoms but also over the sulfur atoms and that the oxidized sulfur atoms exposed outward would easily cause the reactions like S−S coupling or oxidation of solvents.

Acknowledgment. This work was partly supported by a Grant-in-Aid for Scientific Research (No. 03640512) from the Ministry of Education, Science and Culture of Japan. We are very grateful to Prof. S. Nasu for helpful discussions and to Dr. Ishikawa for the use of his pas program.

IC9406493

(30) Takahashi, M.; Watanabe, I.; Ikeda, S.; Kamata, M.; Otsuka, S. *Bull. Chem. Soc. Jpn.* **1982**, *55*, 3757.